Fabrication of astaxanthin-loaded electrospun nanofiber-based mucoadhesive patches with water-insoluble backing for the treatment of oral premalignant lesions

Zhang, Hui; Ji, Yanjing; Yuan, Changqing; Sun, Pei; Xu, Quanchen; Lin, Dongliang; Han, Zeyu; Xu, Xinkai; Zhou, Qihui; Deng, Jing

Published in:
Materials and Design

DOI:
10.1016/j.matdes.2022.111131

Publication date:
2022

Materials & Design 223 (2022) 111131

Contents lists available at ScienceDirect

Materials & Design

journal homepage: www.elsevier.com/locate/matdes

Fabrication of astaxanthin-loaded electrospun nanofiber-based mucoadhesive patches with water-insoluble backing for the treatment of oral premalignant lesions

Hui Zhang [a,b,c], Yanjing Ji [d], Changqing Yuan [a,b], Pei Sun [a], Quanchen Xu [a,b], Dongliang Lin [e], Zeyu Han [a,b], Xinkai Xu [a,b], Qihui Zhou [a,f,*], Jing Deng [a,b,c,*]

[a] Department of Stomatology, The Affiliated Hospital of Qingdao University, Qingdao University, Qingdao 266003, China
[b] School of Stomatology, Qingdao University, Qingdao 266003, China
[c] Dental Digital Medicine & 3D Printing Engineering Laboratory of Qingdao, Qingdao 266003, Shandong, China
[d] University of Groningen, W. J. Kolff Institute for Biomedical Engineering and Materials Science, Department of Biomedical Engineering, University Medical Center Groningen, A. Deusinglaan 1, 9713 AV Groningen, the Netherlands
[e] Department of Pathology, The Affiliated Hospital of Qingdao University, Qingdao University, Qingdao 266003, China
[f] School of Rehabilitation Sciences and Engineering, University of Health and Rehabilitation Sciences, Qingdao 266071, China

HIGHLIGHTS

- Astaxanthin-loaded Janus nanofiber patches were prepared via electrospinning.
- The saliva-insoluble PCL backing prevented drug loss in the oral cavity.
- The patches showed a suitable astaxanthin release rate and permeated into buccal mucosa.
- The patches greatly promoted the recovery of oral premalignant lesions.
- The patches showed great potential for managing oral premalignant lesions.

GRAPHICAL ABSTRACT

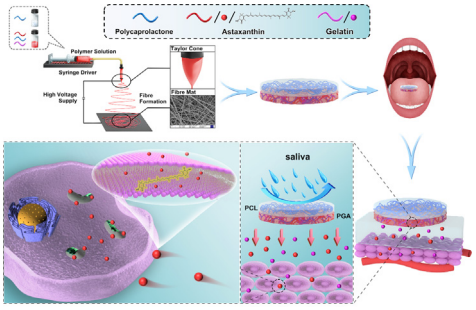

ARTICLE INFO

Article history:
Received 25 June 2022
Revised 6 September 2022
Accepted 6 September 2022
Available online 8 September 2022

Keywords:
Astaxanthin
Electrospun nanofibers
Mucoadhesive patch
Oral premalignant lesions

ABSTRACT

Oral premalignant lesions (OPL) are one of the most common oral diseases, affecting the quality of life and even leading to oral cancer. Current treatments commonly use steroids/retinoids in mouthwashes, films, or ointments. However, conventional drugs/formulations have significant side effects/limitations. Herein, astaxanthin-loaded polycaprolactone (PCL)/gelatin (GT) nanofiber-based mucoadhesive patches (PGA) with the water-insoluble PCL nanofiber backing (PCL/PGA) are developed *via* electrospinning for the management of OPL. The saliva-insoluble PCL backing could greatly prevent drug loss after application in the oral cavity. The prepared PCL/PGA patches exhibit a suitable astaxanthin release rate for achieving high local drug concentration, which permeated into buccal mucosa. In addition, the developed thin patches display excellent wet tissue adhesion and great air permeability due to their high porosity. Notably, the *in vivo* experiment shows that the bioactive mucoadhesive patches significantly promote the recovery of OPL by suppressing the expression of Ki67 and cyclooxygenase-2 (COX-2), comparable to clinical tretinoin cream formulation. Also, the patches did not induce any side effects (i.e., hair loss and oral ulcers) compared to clinical tretinoin cream formulation. The results demonstrate that this novel electrospun mucoadhesive bilayer patch holds great potential for the treatment of OPL.

* Corresponding authors at: Department of Stomatology, The Affiliated Hospital of Qingdao University, Qingdao University, Qingdao 266003, China.
E-mail addresses: qihuizhou@qdu.edu.cn (Q. Zhou), dengjing3333@qdu.edu.cn (J. Deng).

https://doi.org/10.1016/j.matdes.2022.111131
0264-1275/

1. Introduction

Oral squamous cell carcinoma (OSCC) develops from oral premalignant lesions (OPL), which is the most common cancer and constitutes over 90% of head and neck squamous cell carcinoma. According to a recent survey, the overall 5-year survival percentage for OSCC patients is 60%. [1,2] Since the pathophysiology of OPL is not well known, effective clinical therapy is insufficient. There are currently three therapeutic modalities: local or systemic medication therapy, surgery, and phototherapy. [3] Clinical treatment is greatly dependent on steroids/retinoids delivered topically by mouthwashes, films, ointments, or gels due to no trauma, convenient use, direct action, high local drug concentration, and few systemic adverse effects. However, these topical dosage forms are commonly considered suboptimal because of the flushes of saliva, swallowing, and mouth movement, influencing the residence time and drug distribution at the oral lesion location. [4,5] In addition, the steroids/retinoids used for a long time induce unacceptable side effects, leading to the cessation of treatment. Given the above limitations, it is urgent to prepare a novel oral mucoadhesive delivery system that could be loaded with safe and effective natural compounds and firmly adhere to oral mucosa meanwhile accurately administer drugs to the oral lesions for a long time.

Scholars have recently focused on electrospinning as a novel way of producing mucoadhesive patches. [6–9] Electrospinning is a versatile manufacturing technology that produces membranes made of polymeric fibers using a high-voltage electrical current. [10–12] The fiber diameters span from a few nanometers to a few micrometers, which possess a natural extracellular matrix-like structure, highly porous mesh with remarkable interconnection, an incredibly high specific surface area and aspect ratio, sufficient mechanical strength, and favorable biological properties. [13,14] Notably, electrospun fibers have high loading capacity and encapsulation efficiency, making them a highly desirable technique for delivering drugs. [15,16] In addition, careful material selection plays a key role in the success of nanofiber-based mucoadhesive patches. Since its excellent biocompatibility and biosafety, gelatin (GT) is one of the earliest natural tissue engineering scaffolds which can be widely used in regenerating several kinds of tissues. [17–19] Polycaprolactone (PCL), the typical representative of synthetics, is a highly-stable material, exhibiting both good mechanical strength and slow degradation. The electrospun PCL/GT nanofiber system is one of the most intensively researched natural-synthetic hybrid systems. [18] PCL/GT electrospinning fibers system has been widely used in biomimetic engineering for diverse tissues such as skin, [20] dental, [21] nerve, [22] and *et al.* [23,24]. However, whether the PCL/GT electrospinning fibers are suitable for the oral mucoadhesive delivery system is rarely reported.

Astaxanthin (ASX) approved by Food and Drug Administration (FDA) [25] from natural sources has attracted much attention in recent years due to its highest antioxidant ability. [26,27] ASX was discovered in green microalgae Heamatococcus Pluvialis and various marine organisms, and has been used for a variety of therapeutic applications, [28,29] including anti-inflammation, anticancer, and immunomodulatory, antioxidant, *etc.* [30–32] ASX, as a promising agent chemoprevention for OSCC and oral lichen planus (OLP), has also been reported. [33–35] However, ASX is unstable because of its highly conjugated, double bond structure, which induces lower bioavailability and limited use. Previous studies demonstrated that the encapsulation of ASX within nanocarriers enhanced their shelf life, enabled their delivery at the intended site, and increased their physical and chemical stability. [36–38] Therefore, ASX-loaded electrospun GT/PCL nanofiber films (PGA: P-Polycaprolactone, G-Gelatin, A- Astaxanthin) would be an excellent candidate as a mucoadhesive patch for the treatment of OPL, which has not been reported. Besides, to prevent ASX loss from the scour of saliva, the water-insoluble PCL nanofiber backing was designed to combine with PGA. In this work, electrospun PCL/PGA nanofiber-based mucoadhesive patches were fabricated using electrospinning for the management of OPL. The physicochemical properties of nanofibers patches were evaluated by a variety of characterization methods. The wettability of composite mucoadhesive patches was tested by the water contact angle (WCA). The release rate of ASX and its penetration into buccal mucosa were detected. Further, in the OPL rat model, the therapeutic effects and side effects of PCL/PGA mucoadhesive patches and traditional classical drugs on the lesions were observed and compared, and their regulation on the expression of cell proliferation-related antigens Ki67 and cyclooxygenase-2 (COX-2) were analyzed by immunohistochemistry. The ASX nanofiber mucoadhesive patches show great potential in OPL treatment in the future.

2. Materials and methods

2.1. Materials

GT type A (300 Bloom) from porcine skin in powder form, ASX (≥97%), and PCL (Mw = 80,000) were provided by Sigma-Aldrich (USA). Tetramethyl rhodamine isothiocyanate (TRITC)-Phalloidin, and 4′6- diamidino-2-phenylindole (DAPI) solution were obtained from Solarbio (Beijing, China). Artificial saliva and Cell Counting Kit-8 (CCK-8) were purchased from MedChemExpress (Shanghai, China). Dulbecco's modified Eagle's medium (DMEM), fetal bovine serum (FBS), penicillin, and streptomycin were provided by Biological Industries Ltd (Beit-Haemek, Israel). 4NQO was obtained as a powder (Aladdin, Shanghai, China). Pentobarbital sodium and isoflurane were supplied by Youcheng Bio Co Ltd, Hong Kong. Tretinoin cream was purchased from Diwei (Chongqing, China). Ki67 and COX-2 were purchased from Abclonal (USA).

2.2. Fabrication of mucoadhesive patches

2.2.1. Preparation of PGA electrospun membranes

ASX-loaded PCL/GT (PGA) membranes were fabricated by electrospinning. PCL and GT were then dissolved in trifluoroethanol (TFE) in a 50:50 (v: v) ratio at a concentration of 10 wt% and stirred vigorously for 2 h at room temperature. Astaxanthin with different weights was added into the PCL/GT(PG) solution and stirred gently in a light-avoidance condition at room temperature for 4 h to respectively obtain the uniform mixture solution with ASX content of 2.5 and 5 mg. The electrospinning parameters were as follows: 13–16 kV voltage, 1.0 mL/h injection rate, and 15 cm distance between the syringe nozzle and the grounded aluminum plate. All the electrospinning processes were carried out at room temperature (20–24℃) with an ambient humidity of 35–50% on a horizontal electrospinning setup.

2.2.2. Preparation of PCL backing layer

A hydrophobic backing layer was prepared by electrospinning a 10 wt% solution of PCL/TFE on the top of PGA electrospun membranes. Electrospinning parameters were the same as 2.2.1. The PCL/PGA patches were pre-treated in a vacuum oven at room temperature for 48 h before being used in cell or animal experiments.

2.3. Characterization

2.3.1. Scanning electron microscopy (SEM)

The surface morphologies of fibrous samples were observed by SEM (Zeiss, SIGMA, Germany). Samples were sputter-coated with

gold and imaged using an emission current of 15 kV. Using the Image J software, the average diameter of the fibers was calculated by measuring at least 100 fiber segments from three different SEM images for each type of sample.

2.3.2. The analysis of ASX content

The ASX content was then analyzed using high-performance liquid chromatography (HPLC) (LC-20A, Japan). Firstly, PGA samples were purified twice by submerging an accurately weighed membrane (0.05 mg) in 20 mL of acetone. And then 2 mL sample solution was taken and added methanol to a constant volume of 5 mL. A diamond plus C18 column (250 × 4.6 mm, 5 μm particle size) was used. A total of 20 μL of the immersing solution were injected and examined by HPLC, which was done according to a previously published method with minor changes. [39] The amount of ASX in the membranes was calculated by the standard curve for ASX.

2.3.3. ATR-FTIR analysis

Attenuated total reflection Fourier transform infrared spectroscopy (ATR-FTIR) was performed over the range of 500–4000 cm^{-1} at a scanning resolution of 2 cm^{-1} during 32 scans using a Nicolet in10 FTIR spectrometer (Thermo Fisher Scientific, Waltham, MA, USA).

2.3.4. XPS analysis

X-ray photoelectron spectroscopy (XPS) was determined by an X-ray electron spectrometer (Thermo Fisher ESCALAB XI+, Waltham, MA, USA) by Al Kα radiation. The XPS Peak 41 software was used to record the full-scale XPS survey spectra to confirm the incorporation in each procedure.

2.3.5. XRD analysis

X-ray diffraction analysis (XRD) of the electrospun membranes samples and ASX analytical standard were performed using a DX2700 spectrometer (D8 Advance, Bruker, ASX, GmbH, China). All samples were analyzed from 5 to 80° (2θ) by using Cu radiation at the scan parameters: scanning rate 5° (2θ)/min, voltage 40 kV, and current 40 mA.

2.3.6. WCA analysis

WCA on the PGA, PG, and PCL electrospun membranes were determined using a video-enabled goniometer (Theta, Biolin, Sweden). 5 μL water was automatically dropped onto the flat electrospun samples. The WCA was immediately measured on both sides of the droplet automatically, which indicated the wetting ability of the materials. All measurements were repeated at least three different positions of each sample, and the results were averaged.

2.4. In vitro drug release

The PGA electrospun membranes (2.5 and 5 mg) were immersed in artificial saliva for 2 h. Then, the surface morphology was observed by SEM after natural drying. The PGA electrospun membranes (2.5 and 5 mg) were immersed in 20 mL of artificial saliva (pH = 6.8) at 37 °C. The artificial saliva medium was stirred at a constant rate of 100 rpm and the solution sample (10 mL) was removed and replaced with an equal volume of fresh pre-warmed fluid at pre-determined intervals (15–480 min). The amount of ASX in the samples of dissolution fluid was analyzed by an Ultraviolet spectrophotometer (YuanXi, Shanghai, China) regarding the previously standard curve ($r^2 > 0.99$).

2.5. Ex vivo drug permeation studies

Ex vivo drug permeation testing was conducted using porcine buccal tissue since it is considered to have a closer resemblance to human buccal mucosa than other animal tissues. [40] Mucosa (2 × 2 cm) were affixed in a Franz cell (6.5 mL receiver volume of fluid), exposure area of 2.2 cm^2, 37 °C, wetted with artificial saliva (50 μL), and PGA patches (1.5 × 1.5 cm) applied with gentle pressure to the mucosal surface. The patches were removed at pre-determined times (0.5, 1, 1.5, 2 h), and a 1 mL sample solution of the acceptor buffer was collected. To calculate the amount of drug within the mucosa, the mucosa pieces were removed from the epithelial layer of the mucosa, which were subsequently cut into smaller pieces and placed in acetone (1 mL) and treated with ultrasound for 10 min before filtering for analysis. Both the collected receiver buffer and acetone were analyzed for the concentration of ASX by HPLC (as 2.3.2).

2.6. In vivo residence time of PGA electrospun membranes in rats

Ten male SD rats (6 weeks old) were purchased from Jinan PengYue Experimental Animal Raising Farm (Jinan, China). All experimental protocols were approved by the Animal Care and Use Committee of Qingdao University, following the instructions (Laboratory animal use license number:20200829C576J701118002). A study was performed to determine experimental residence time. PGA electrospun membranes were applied to the tongues of ten anesthetized rats and the electrospun membranes were visually examined for electrospun membrane detachment for up to 120 min. The time was recorded when the electrospun membrane had completely detached from the mucosa as the residence time.

2.7. Cell culture

Oral mucosal tissue blocks obtained during the extraction of the third molar (Stomotolgy, The Affiliate hospital of Qingdao University) were treated with the modified tissue culture, and the primary human gingival fibroblasts (hGFs) were extracted for primary culture and passed to the third generation for the later experiment. The patient's informed consent has been approved by the Ethics Committee of the Affiliated Hospital of Qingdao University (The number: QYFY WZLL 27015), China. In addition, hGFs were extracted and identified in our previous work. [41].

2.7.1. Cell adhesion assay

Before cell inoculation, each group (PG, 2.5% PGA, 5% PGA) of samples in the 24-well plate was sterilized under ultraviolet irradiation for 1 h, and then soaked in PBS solution for 2 times, 2 min each time. The digested suspended hGFs were diluted to a suitable concentration and planted on the samples at a density of 5 × 10^3 cells/well for 1 d. First, the cells were fixed at room temperature with 4% paraformaldehyde for 30 min, and then permeated with 0.5% TritonX-100 solution for 5 min to make the cell membrane permeable. Finally, the nuclei were stained with 4′-6-diamino-2-phenylindole (DAPI), and actin was stained with Rhodamine-Phalloidin. Three samples in parallel in each group were observed the adhesion of cells to the fibers using Fluorescence Microscopy (Nikon A1 MP, Japan). Finally, the cell density, single-cell spreading area, and cell elongation were quantitatively analyzed with Image J.

2.7.2. Cell proliferation test

The viability of hGFs on different samples was assessed by CCK-8. After 1 and 2 d of cell-material co-culture, the cells were washed with PBS solution to remove unadhered cells. Then 30 μL CCK-8 and 270 μL complete medium were added to a 24-well plate and

incubated in a carbon dioxide incubator for 1 h. Two copies of 150 μL incubated solution were taken from each sample and added to the 96-well plate. The absorbance was measured at 450 nm with a microplate analyzer (Bio Tek, Synergy TMH1/H1M, USA) (n = 6 in each group).

2.8. Animal experiment

Sixty-five male SD rats (4 weeks old) were purchased from Jinan PengYue Experimental Animal Raising Farm (Jinan, China). All experimental protocols were approved by the Animal Care and Use Committee of Qingdao University, following the instructions (Laboratory animal use license number:20200 829C576J701118002). After a week of acclimation, the rats were separated into experimental groups (n = 60, 5 per cage) and a control group (n = 5) randomly in separate cages.

The rats in the experimental groups were treated with 0.002% 4NQO in the drinking water, while the rats in the control group were treated with normal drinking water. The treatment lasted for 12 weeks to obtain the OPL model. Gross lesions were identified and photographed after 4NQO treatment at 8 and 12 weeks. Two rats were sacrificed respectively at the above two-time points. The sections from the tongues were deparaffinized, rehydrated, and stained with H&E for histopathology.

The rats in the experimental groups were randomly divided into six groups. Two groups (n = 10) were respectively treated with 2.5% PGA membranes and VA ointment when they continued to drink 4NQO solution, and two groups (n = 10) were treated as above when they stopped drinking 4NQO solution. Both the continued drinking 4NQO solution and stopped drinking 4NQO experiment groups, all had a control group (n = 5) without any treatment (Fig. 1).

Each group was given intraperitoneal anesthesia with pentobarbital sodium at a fixed time by four fixed experimenters every day, combined with isoflurane inhalation anesthesia. The anesthesia time was maintained for 1.5–2 h after the corresponding drug treatment. During the experiment, the changes in white lesions' color and shape were observed every day, and the photos were kept regularly. The rats' blood samples were collected from the apex of the heart under anesthesia and the tongues were resected on the 28th d under anesthesia. Then rats were euthanized. Blood samples were centrifuged at 3000 rpm to take the upper serum, and triglyceride, high-density lipoprotein, and cholesterol were measured. The tongues were immediately fixed in 10% neutral-buffered formalin solution for 12–24 h and paraffin embedded. Two 4-μm-thick sections in each group were mounted on glass slides, respectively treated for Ki67/COX-2 immunohistochemical labeling.

2.9. Data analysis

Each set of data was presented as mean values with standard deviation (SD). GraphPad PRISM 8.0 was used for statistical analysis. The student's *t*-test was used to determine the differences between two groups of data. The error bar indicates the SD of triplicate measurements over each group. Asterisks represent significant difference in the data at $^{*}p < 0.05$, $^{**}p < 0.01$, and $^{***}p < 0.001$.

3. Results and discussion

3.1. Preparation and characterization of PCL/PGA mucoadhesive patches

As shown in the lower-left macrograph of Fig. 2**A**, the electrospun PGA nanofiber membranes turned red due to the addition of ASX, and their color gradually became darker with the increased concentration of ASX. As presented in Fig. 2**A/ii**, 2.5% PGA nanofibers were smooth, uniform, and fine, which indicates that the ASX was well incorporated within the fibers and had no effect on the electrospinnability of the solution. However, as shown in Fig. 2**A/iii**, the 5% PGA membranes had scattered insoluble particles with the increase of ASX probably owing to the inhomogeneous solution or phase separation, resulting in deteriorated fiber morphologies (e.g., splash, fiber bonding, and varied fiber size) over time during electrospinning. [18] The diameters of the nanofibers were analyzed with Image J software. Fibers with varied ASX mass concentrations of 0, 2.5%, and 5% were measured to be 466 ± 245, 592 ± 279, and 707 ± 258 nm, respectively. It implies that the prepared nanofiber diameters increased with an increased amount of ASX. To prevent drug removal by flowing saliva, the hydrophobic PCL backing layer was prepared on the PGA film. The PCL electrospun nanofibers also possessed smooth morphology and uniformly diameter distributions as shown in Fig. 2**A/iiii**.

Further, HPCL was employed to detect actual amounts of loaded ASX. The data in the 2.5% PGA group reveals their drug content (2.43 ± 0.11%) was slightly lower than the loaded dose (Fig. 2**B**). The ASX content (3.4 ± 0.18%) detected in the electrospun membrane of the 5% PGA group was significantly lower than that added, probably because ASX powder could not completely be dissolved in the

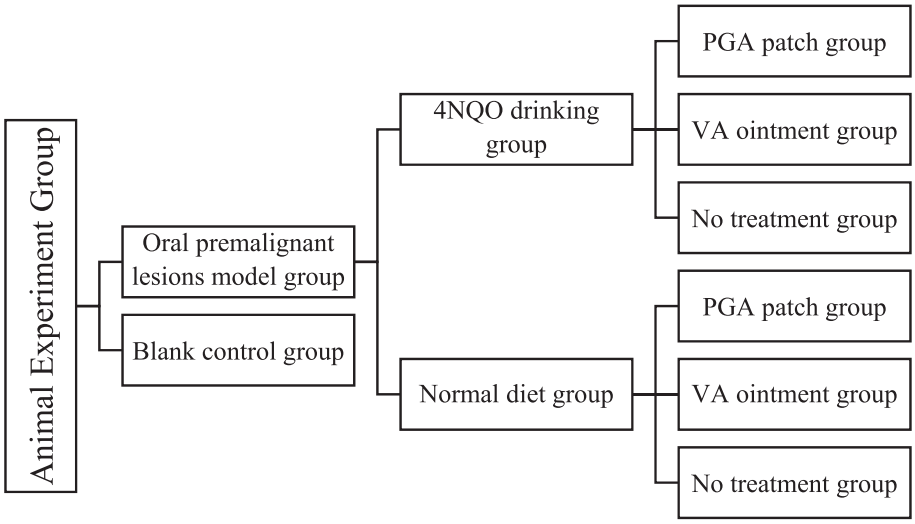

Fig. 1. Schematic diagram of animal experiment groups.

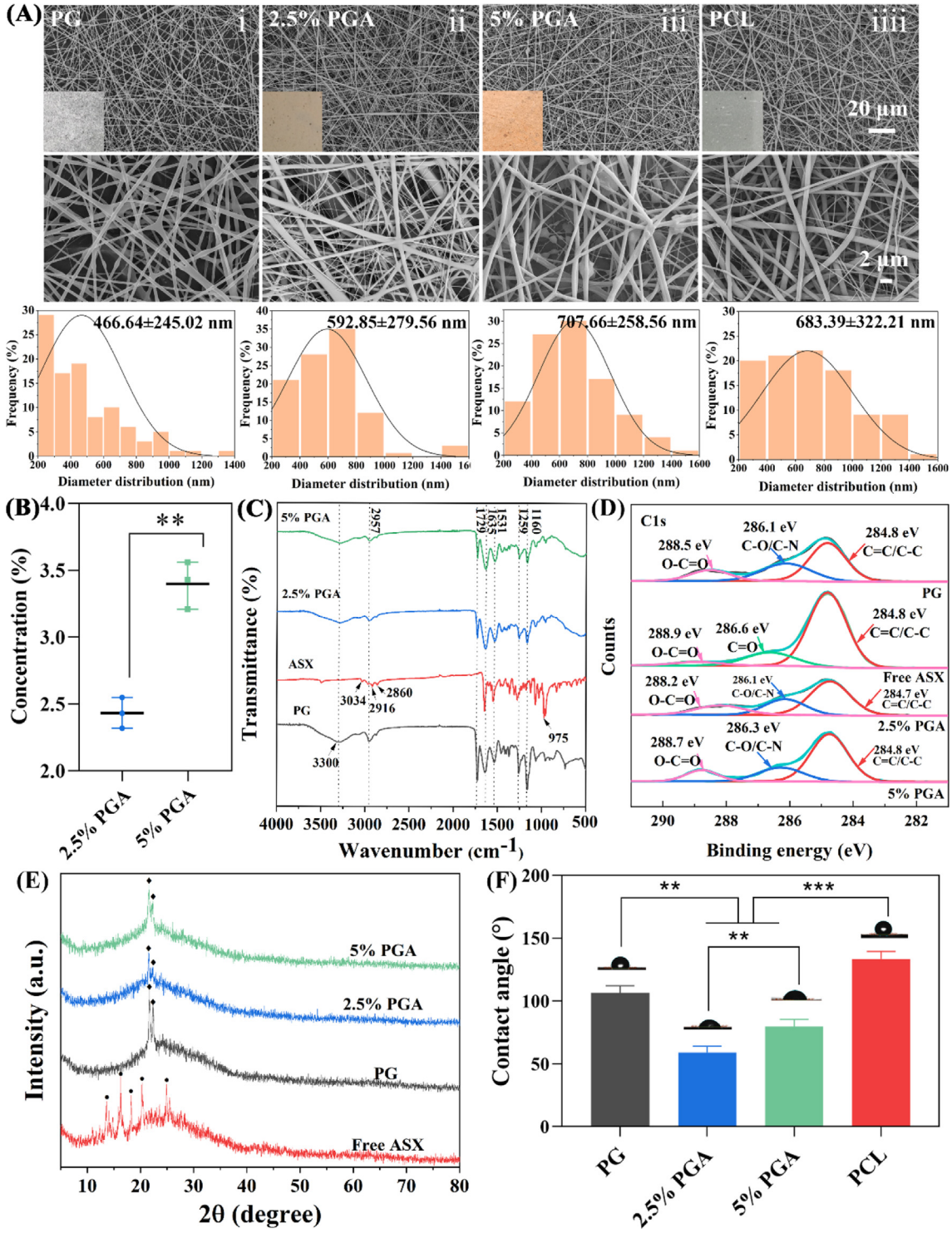

Fig. 2. (A) SEM images and diameter distribution of the electrospun nanofibers. The insets in SEM images are the photos of corresponding electrospun membranes. (B) Actual ASX content loading in PGA electrospun membranes (2.5% and 5%). (C) FTIR spectra, (D) XPS survey spectra and (E) XRD patterns of PGA electrospun membranes (0, 2.5% and 5%) and ASX powder. (F) WCA of water droplets on different PGA and PCL membranes at 1 s.

polymer solution. The results suggest that ASX was successfully loaded into the PG nanofibers and uniform morphology of electrospun nanofiber film was prepared.

To identify the functional groups and molecular interactions in composite nanofibers, FTIR spectra of ASX powder and PGA electrospun membranes were measured. As shown in Fig. 2**C**, in the spectrum of the PG group, the typical peaks at 3300 and 2957 cm^{-1} were attributed to the stretching vibration of the $-NH_2$ and –OH as well as the asymmetric stretching of $-CH_2$, respectively. In addition, the absorption peak at 1635 cm^{-1} was the C=O tensile vibration, belonging to the amide I bond, the absorption peak at 1531 cm^{-1} was the N-H bending vibration of the amide II bond, and the absorption peak at 1259 cm^{-1} represented the C-N tensile vibration of the amide III bond. [42,43] In the spectrum of ASX, 3034 cm^{-1} was the middle O-H stretching vibration peak, 2972 cm^{-1} was the *trans*-olefin –CH=CH– vibration peak,

2916 cm^{-1}, and 2860 cm^{-1} were the asymmetric and symmetric stretching peaks of $-CH_2$, and 1635 cm^{-1} was the C=O vibration peak. [30,44] From comparison in the spectra, it showed that the surface of PGA electrospun membranes did not contain the characteristic peak of free ASX, indicating that not much ASX was exposed to the surface of electrospun membranes and most of them were encapsulated in the PG nanofiber system, which could not only prevent the loss of ASX bioactivity caused by light and oxidation but also maintain its sustained release. [45,46] It was reported that [47–49] polymeric/biopolymeric nano vehicles (nanoparticles, nanogels, nanotubes, and nanofibers) originated from biodegradable and biocompatible materials are promising candidates for targeted delivery of carotenoids (ASX as a xanthophyll carotenoid [50]).

The elemental composition of the electrospun nanofiber membranes was analyzed by XPS. The full-scale XPS survey spectra were recorded to further confirm the incorporation in each procedure (Fig. 2**D**). The atomic ratio of carbon, nitrogen, oxygen, and chemical bond of PG nanofibrous films before and after ASX loading calculated from XPS survey scan spectra were summarized. The PG nanofibrous films exhibited typical peaks at 284.8, 286.1, and 288.5 eV, which were attributed to C=C/C-C, C-O/C-N, and O-C=O bonds, respectively. After ASX loading, the peak at 286.6 eV (C=O) of free ASX was not detected on 2.5% and 5% PGA nanofibrous films. It suggests most of ASX was encapsulated in the PG nanofiber because only ASX on the material surface could be detected by XPS. [51] This result was in line with the results of FTIR.

The crystallographic structure of the ASX powder and electrospun PGA membranes was determined by XRD analysis. As presented in Fig. 2**E**, the diffractogram of ASX powder exhibited characteristic peaks (i.e., 13.62°, 16.28°, 18.22°, 20.24°, and 24.84°), indicating that ASX was presented in crystalline form. Moreover, corresponding peaks disappeared in the diffractograms of ASX-loaded electrospun membranes, confirming that the interaction of ASX with PG caused a remarkable decrease in crystallinity. The result reveals that ASX was well incorporated into the electrospun membranes and converted from its crystalline state to an amorphous state. In addition, the lower crystallinity of a component material indicated the great miscibility of blended nanofibers. [52].

The surface free energy or wettability of PGA electrospun membranes was evaluated by measuring the dynamic WCA (Fig. 2**F/S1**). The PG electrospun membranes exhibited greater WCA (112.93 ± 2.13°, 1 s) compared to PGA groups. And the WCA of PG electrospun membranes slowly decreased within 30 s from 112.93° to 83.46°. After adding ASX, the WCA significantly reduced compared to the PG group, especially in the 2.5% concentration group (57.95 ± 1.25°, 1 s). The spherical shape of the water droplet could not retain on the 2.5% PGA electrospun membrane (disappeared quickly within 30 s), suggesting much better wettability than PG and 5% PGA groups. The results revealed that 2.5% PGA electrospun membranes had better hydrophilicity which might be more beneficial to drug release and better integrated with the tongue. Furthermore, the WCA on PCL electrospun membranes (140.57 ± 2.56°, 1 s) indicates that the surface of the backing layer was hydrophobic. This wettability feature was maintained steadily over time (**Figure S2**). This result showed a dual-layer oral mucosal patch was successfully fabricated, which could be poorly wetted in the oral cavity and greatly prevent drug loss after application. [6].

3.2. ASX release and permeation assessment

After electrospun PGA nanofiber membranes were soaked in artificial saliva for 2 h, their surface morphology was observed by SEM. As expected, the nanofibers were partially dissolved (Fig. 3**A**) owing to the dissolution of GT in the nanofiber membrane. The undissolved part was the PCL which acts as mechanical support. Electrospun nanofiber affords great flexibility in selecting materials for drug delivery applications. The polymer composition of electrospun membranes is crucial in determining drug release kinetics [53–56]. Either biodegradable or non-degradable materials can be used to control the rate of drug release *via* diffusion and degradation. [57].

The cumulative percentage of ASX released from PGA electrospun membranes versus time was displayed in Fig. 3**B**. No difference was observed in the ASX release profile between 2.5% and 5% PGA samples. All the ASX-loaded electrospun membranes released the ASX in a sustained manner over a 10 h period, with approximately 60% released after 120 min. ASX continued to be sustained release, reaching 70% within 600 min. It is a positive behavior to release a massive burst of ASX from oral patches in less than 2 h for the local application. This result demonstrates that *in vitro* release profiles of PGA samples could achieve high local drug concentration in a short time mainly owing to the dissolution of GT. The excellent release of ASX from the nanofiber films was also caused by the high surface area and porosity of the electrospun membranes, [58] which is suitable for local drug use.

In vitro drug permeation test, where conditions are as similar as possible to *in vivo* conditions (Fig. 3**C**), is a valuable study to be conducted to determine the expediency of employing a particular drug or drug delivery system for buccal administration. [59] Since the 2.5% PGA group was not significantly different from the 5% PGA group in the drug release, 2.5% PGA electrospun membranes were selected in the following experiment. ASX in 2.5% PGA electrospun membranes permeating into *ex vivo* porcine mucosa was investigated for 2 h. HPLC analysis reveals that the released ASX was able to permeate into porcine buccal mucosa within 0.5 h and in a time-dependent manner (Fig. 3**D**).

To investigate *in vitro* and *vivo* residence time of electrospun membranes, the flow-through method and animal experiments were performed. [60,61] The electrospun membranes adhered firmly to the pigskin *in vitro* and did not fall off underwater washing (Fig. 3**E**). Further, *in vivo* tests demonstrated that PGA electrospun membranes could maintain close fitting with the tongue mucosa of SD rats (Fig. 3**F**) and it could continue to adhere for an average time of approximately 120 ± 45 min (Fig. 3**G**).

Due to the moist mucosal surfaces, salivary flow, and motion within the oral cavity, controlled delivery of drugs to the oral mucosa is challenging. Although the high surface area/volume ratio of electrospun fibers is a potentially attractive feature for drug delivery at site-specific, this approach is based on the fibers could firmly adhere to the mucosal surface first. The results shown here demonstrate that the combination of drug-loaded electrospun fibers with a hygroscopic polymer facilitates long-term adhesion that further leads to successful local delivery of ASX. This work demonstrated the usefulness of PGA electrospun fibers to address the challenge of topical drug delivery to mucosal surfaces, including within the oral cavity.

3.3. Cytocompatibility assessment

It is critical to evaluate whether biomaterials are suitable for biomedical applications by measuring their cytocompatibility. [62,63] HGFs were chosen as the model cell type, which were representative cells in the oral mucosa. HGFs were co-cultured with PGA samples to confirm their biocompatibility using detecting cell adhesion and viability. The behavior of cell adhesion (morphology change, recruitment, proliferation, and differentiation) has been considered to be a critical premise for the subsequent interactions between biomaterials and cells. [64,65]

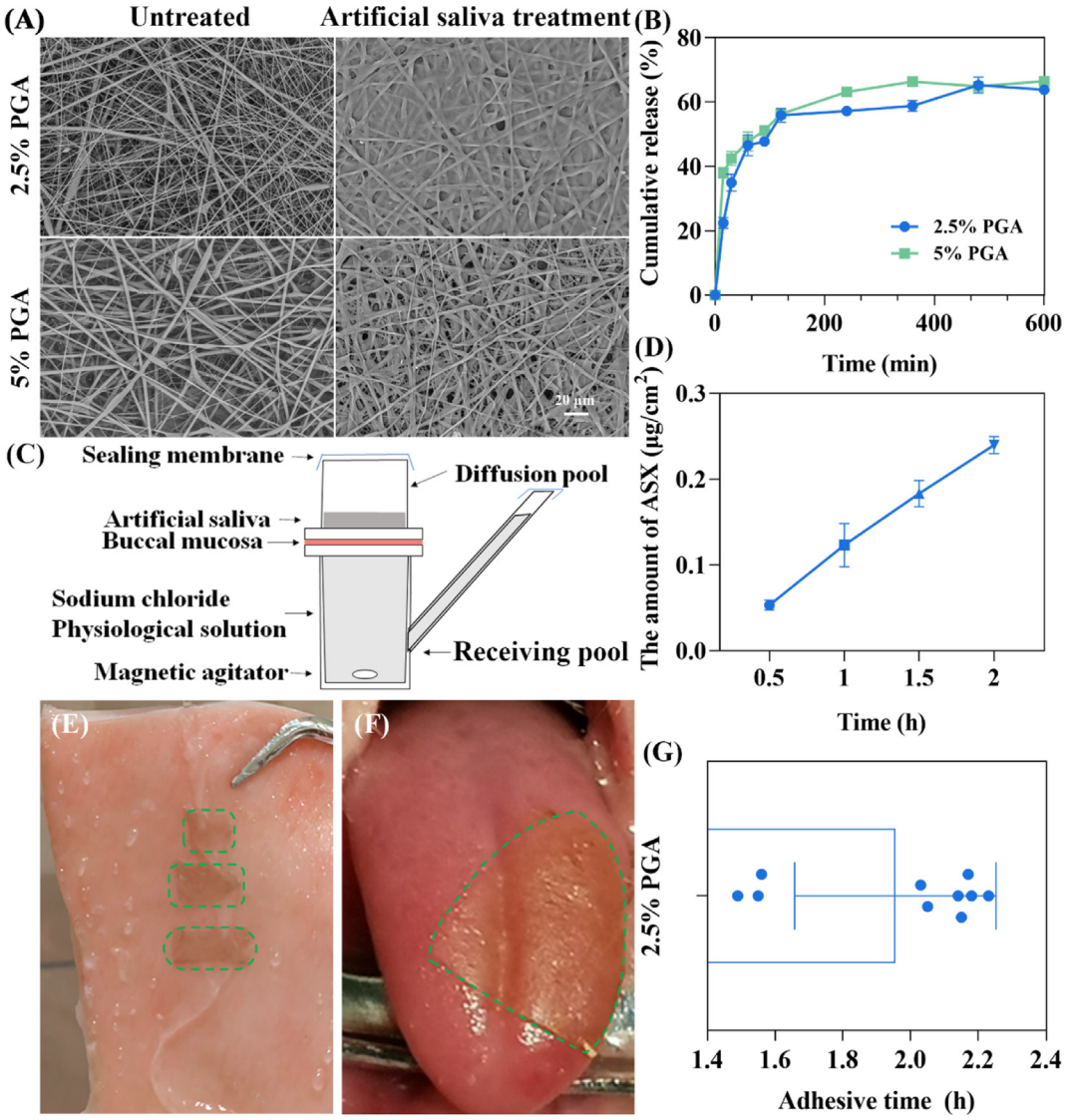

Fig. 3. (A) The change of fiber morphology after PGA electrospun membranes were soaked in artificial saliva. (B) The release profiles of ASX from PGA electrospun membranes. (C, D) The ASX from 2.5% PGA electrospun membranes permeating into porcine buccal mucosa. (E) Photograph of 2.5% PGA electrospun membranes adhered to pig skin and washed by flowing water. (F) Photograph of 2.5% PGA electrospun membranes adhered to the tongue mucosa of SD rats and (G) average residence time (n = 10).

HGFs adhesion after 1 d was observed by the double-label fluorescence staining of the actin cytoskeleton (red) and nucleus (blue). The inoculated hGFs cells in all the groups showed representative spindle-like morphology **(**Fig. 4**A)**. Quantification confirms that in electrospun membrane groups, there was no significant difference in cell density (Fig. 4**B**), but cell elongation increased (Fig. 4**C**) and cell spreading area decreased significantly (Fig. 4**D**) compared to the blank group. It may be due to the addition of ASX in the developed nanofibers.

Cell viability on electrospun membranes was measured by a CCK-8 assay after 1 and 2 d of cell culture. As data revealed in Fig. 4**E**, the cell viability with all electrospun membrane groups had no significant difference after 1 d of cell culture. After 2 d of cell culture, the differences among the groups were statistically significant. The electrospun membranes loaded with different concentrations of ASX were significantly higher than the PG group. The results of the cell attachment analysis and CCK-8 assay all suggested the excellent cytocompatibility of the PGA electrospun membranes. It is reported that the ability of electrospun nanofibers to mimic the extracellular matrix (ECM) is crucial because both the size scale of the structure and the morphology respectively play essential roles in cell proliferation and adhesion. [66–68] In addition, electrospun membranes comprised of nanofibers are considered an ideal material for cell attachment as they have a very high fraction of surface available to interact with cells. [69,70] This further confirmed the advantages of using electrostatic spinning technology loaded ASX to produce an oral mucosal patch in this study.

3.4. Evaluation of in vivo therapeutic efficacy

To evaluate the therapeutic efficacy of PGA electrospun membranes *in vivo*, rat OPL model and treatment tests were carried out. Based on the above physicochemical and biological features of prepared PGA electrospun membranes, 2.5% PGA was chosen to perform the following therapeutic efficacy experiment. Meanwhile, a clinical tretinoin cream (VA) was selected as the positive therapeutic drug for comparison.

The procedure of the animal experiment is shown in Fig. 5**A**. Firstly, the rat OPL model was obtained in 12 weeks. As shown in Fig. 5**B**, after 8 weeks of 4NQO treatment, scatter non-detachable white lesions were visible on the dorsal sides of the tongues, and

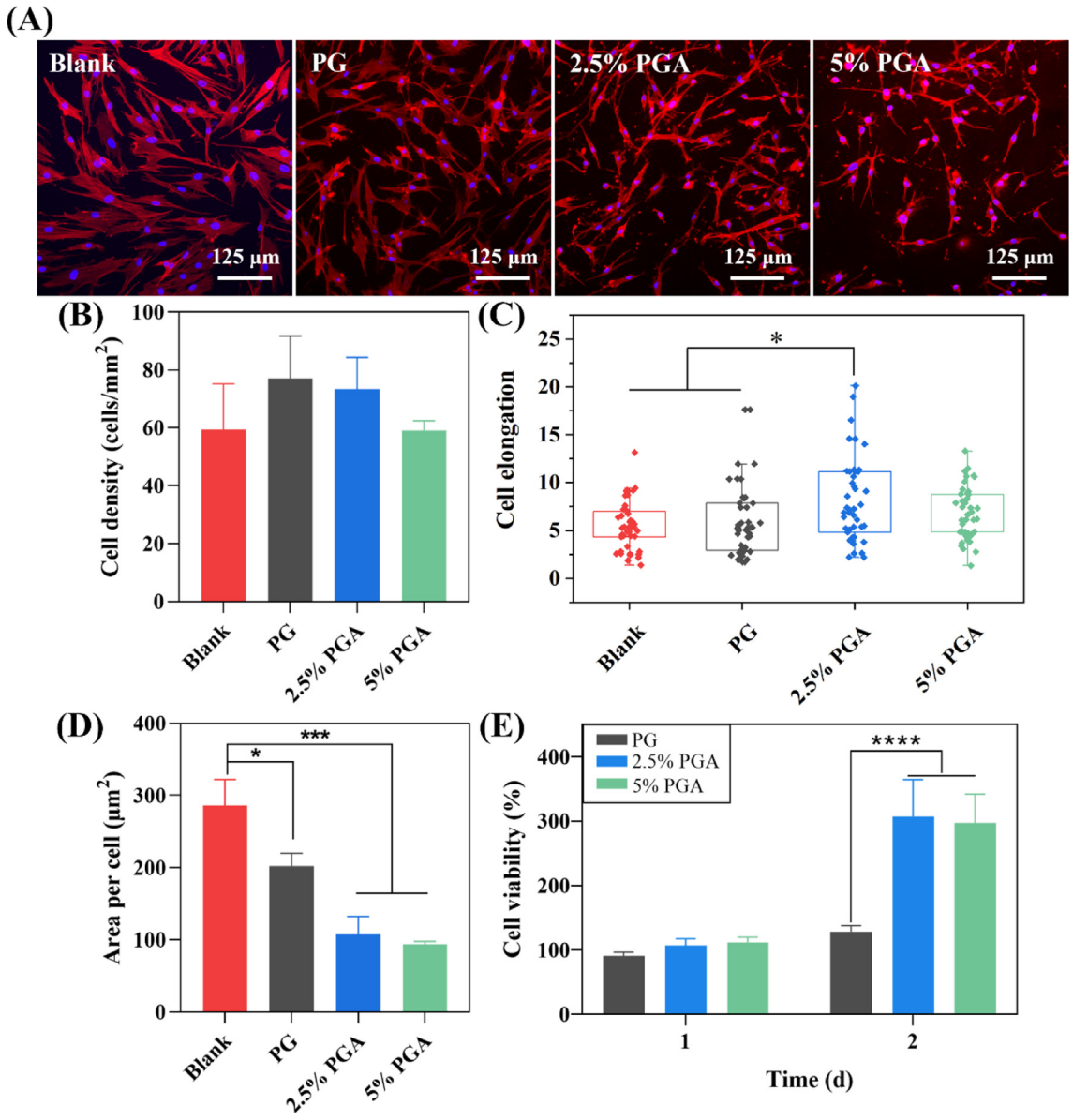

Fig. 4. (A) Fluorescent images of hGFs co-cultivation with the electrospun membranes containing different content of ASX for 24 h. (B–D) Cell density, elongation, and area per cell of hGFs co-cultivation with the electrospun membranes containing different content of ASX for 24 h. (E) Cell viability of hGFs after incubation with the electrospun membranes containing different content of ASX.

the white lesions were more evident at 12 weeks. No severe lesions were observed in other areas of the mouth, because the upper surface of the tongue is the area of the mouth that had the most exposure to 4NQO water. [71] Histologically, tongues from the control group showed a very clearly defined epithelium with a single layer of basal cells. OPL mucosa of rat tongues was observed to possess focal areas of mild epithelial hyperplasia after 4NQO-treated 8 weeks. The epithelium was thickened and hyperkeratotic, its projections were irregular and blunt, and basal hyperplasia was observed after 4NQO-treated 12 weeks (Fig. 5**B**). Therefore, the animal model of OPL was established successfully.

The lesions of treatment groups (i.e., 2.5% PGA and VA) and control groups were observed for a period of 14 and 28 d post-treatment, respectively (Fig. 5**C**). When the rats drank normal water, white lesions on the tongue of rats became lighter, smaller, or even disappeared, which was treated by both PGA and VA. There was no visible change in the control group with no treatment. The result indicates that the removal of 4NQO stimulation alone did not upturn the lesions, but two treatments after the removal of 4NQO stimulation achieved a good therapeutic effect. When the rats continued to drink 4NQO solution, the white lesions on the tongue were not a significant change for the better in either PGA or VA treatment groups. However, two out of six rats in the VA group developed severe oral ulcers. Meanwhile, the lesions were observed to significantly increase in the number and area in the control group with no treatment. The results reveal that while rats continued to drink 4NQO solution, the lesions developed seriously without any treatment, but both treatment groups had similar control over the progression of the disease. It was worth noting that there were significant side effects in the VA group.

To further confirm the therapeutic efficacy, immunohistochemical analysis of Ki67 and COX-2 was performed on the tissues. The nuclear Ki67 antigen is a recognized objective marker of tumor proliferative activity. It is a nuclear non-histone protein that is nor-

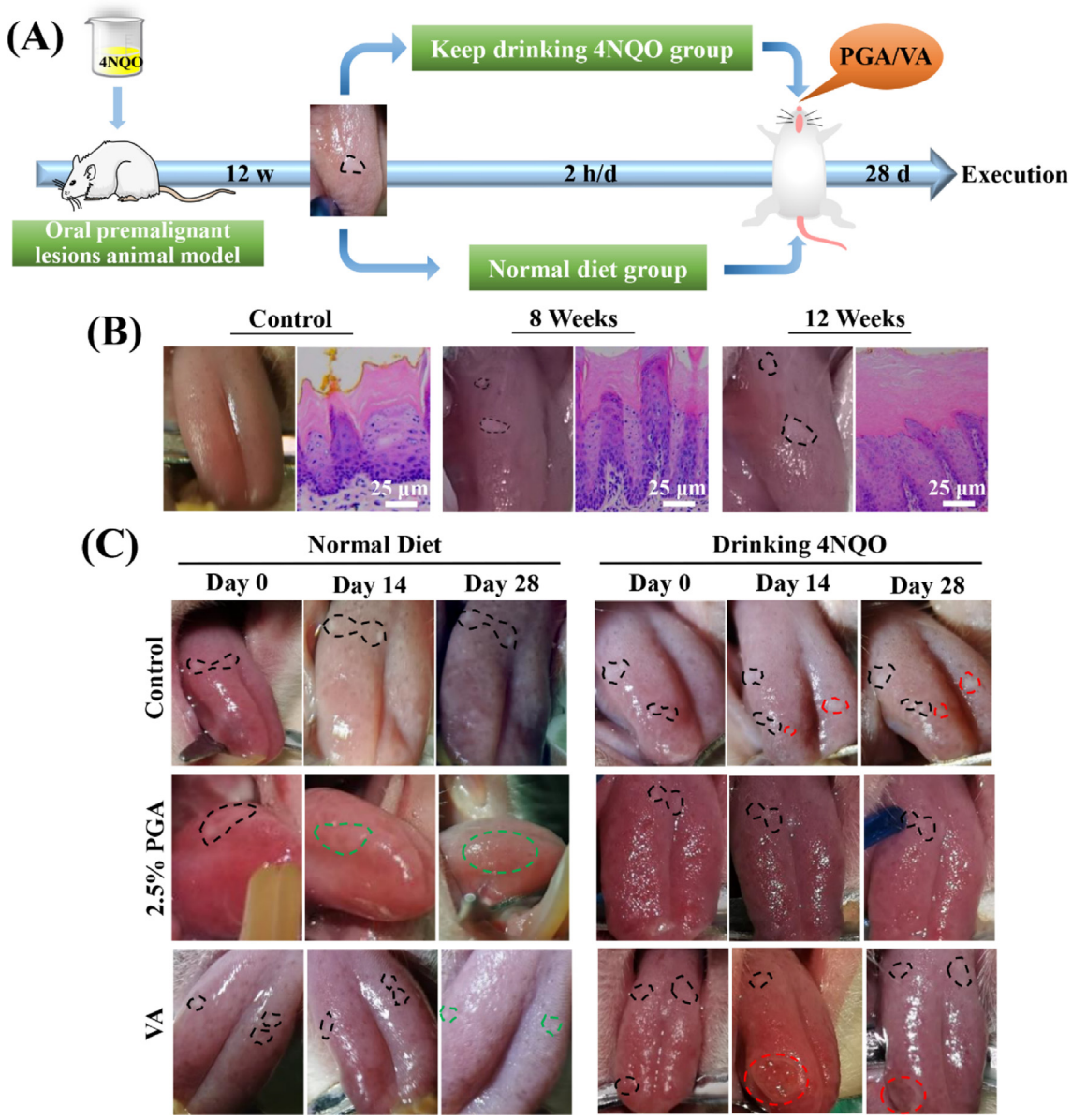

Fig. 5. (A) Schematic diagram of the animal experiment. (B) Photographs and HE images of rat tongues after drinking 4NQO solution 0, 8, and 12 weeks. (C) Photographs of OPL treated by PGA electrospun membranes and VA-ointment at 0th, 14th, and 28th d (the green dotted line means better therapeutic effect; the red dotted line means worsen therapeutic effect; the black dotted line means no change). (For interpretation of the references to color in this figure legend, the reader is referred to the web version of this article.)

mally expressed in proliferating cells but not in quiescent cells, which has been widely used as the prognostic marker in numerous cancers. [72,73] Either in the normal diet group or drinking 4NQO group, on 28th d, the expression of Ki67 protein in the two experimental groups was significantly lower compared with control groups without any treatment (Fig. 6**A**).

COX-2 is rarely expressed in the normal epithelium but is highly expressed in OSCC tumors and the surrounding lymphocytic infiltrates. [74,75] Further support was found on an increased level of COX-2 in OPL compared with oral hyperplastic epithelium, suggesting that COX-2 is involved in the early stages of oral carcinogenesis. [76] Either in the normal diet group or drinking 4NQO group, on 28th d, the expression of COX-2 protein in the two experimental groups was greatly decreased compared with control groups without any treatment (Fig. 6**A**).

The quantitative analysis of the immunohistochemical images by Image J was shown in Fig. 6**B**. In the normal diet group, the expression of Ki67 and COX-2 in both treatment groups was significantly lower than in the untreated group ($p < 0.001$). The expression of Ki67 was also significantly decreased in the no-treatment control group ($p < 0.01$), but not as apparent as that in the two treatment groups. In the 4NQO drinking group, the expression of Ki67 ($p < 0.05$) and COX-2 ($p < 0.001$) in two treatment groups were significantly reduced, while the expression of Ki67 and COX-2 in the no treatment control group was significantly increased ($p < 0.001$).

Taken together, when the pathogenic factors were removed in OPL rats, both PGA electrospun membrane and commercial Tretinoin cream showed excellent therapeutic efficacy by mediating cell proliferation. And while the pathogenic stimuli of OPL rats per-

sisted, both PGA electrospun membrane and commercial Tretinoin cream also could control the deterioration of OPL disease by regulating cell proliferation. The above results display that the therapeutic effect of the 2.5% PGA electrospun patch was significantly comparable to the clinical tretinoin cream formulation.

3.5. Safety and side effects

The use of VA in clinical practice is limited as long-term administration of VA is associated with toxicity manifested by hepatic and lipid changes, oral dryness, hair loss, teratogenicity, and bone and connective tissue damage. [77] In this animal experiment, the side effects (i.e., hair loss and oral ulcers) were also observed in some rats treated with VA ointment (Fig. 7**A**). And water intake per day of rats in the VA group was significantly higher than the control and 2.5% PGA electrospun membrane groups (Fig. 7**B**). This result implied that the rats who used VA ointment might feel oral dryness.

The blood test results (**Figure S2**) of the VA ointment treated rats in the drinking 4NQO group showed that total cholesterol and triglycerides were significantly increased compared with the control group and 2.5% PGA group, while the high-density lipoprotein was decreased considerably. This result is consistent with the previous report that retinoids lead to an increase in the levels of triglycerides and total cholesterol and a decrease in the high-density lipoprotein levels. [78] Nevertheless, the blood test results in the regular diet group were not corroborated with it. The difference in the regular diet group may be due to the shorter duration of drug use (28 d). The abnormal lipid metabolism in the drinking 4NQO group may be caused by long-term consumption of 4NQO solution leading to rats so weak that short-term local application of VA ointment could affect lipid metabolism. It cannot be ruled out that long-term use of 4NQO solution might lead to abnormal lipid metabolism. However, it was determined that the 2.5% PGA group did not show any abnormalities in lipid metabolism, although the rats continued to be treated with 4NQO solution.

It is well known that ASX is safe without side effects. Also, ASX showed potential anti-ulcer properties in murine models as reported by Murata *et al.* [79] Therefore, ASX had great potential as an oral topical drug. In this study, when ASX was loaded into the PGA nanofiber patch by electrospinning and applied to OPL, there was also no side effect. The result showed that 2.5% of PGA electrospun membrane possessed better safety compared with traditional medicine like VA ointment.

4. Conclusions

In summary, bioactive PCL/PGA nanofiber-based mucoadhesive patches with water-insoluble backing were successfully developed *via* electrospinning technology for the management of OPL. The PCL backing was poorly wetted in the oral cavity, which could greatly prevent ASX loss in practical applications. The PCL/PGA mucoadhesive patches are firmly attached to the oral mucosa under flowing saliva for more than 2 h. The developed patches displayed a suitable ASX release rate for achieving high local drug concentration, which permeated into buccal mucosa. Also, the prepared mucoadhesive patches exhibited satisfactory cytocompatibility. Furthermore, the *in vivo* experiment demonstrated that the 2.5% PGA mucoadhesive patches significantly promoted the recovery of OPL by suppressing the expression of Ki67 and COX-2 in the OPL rat model, which was comparable to clinical tretinoin cream

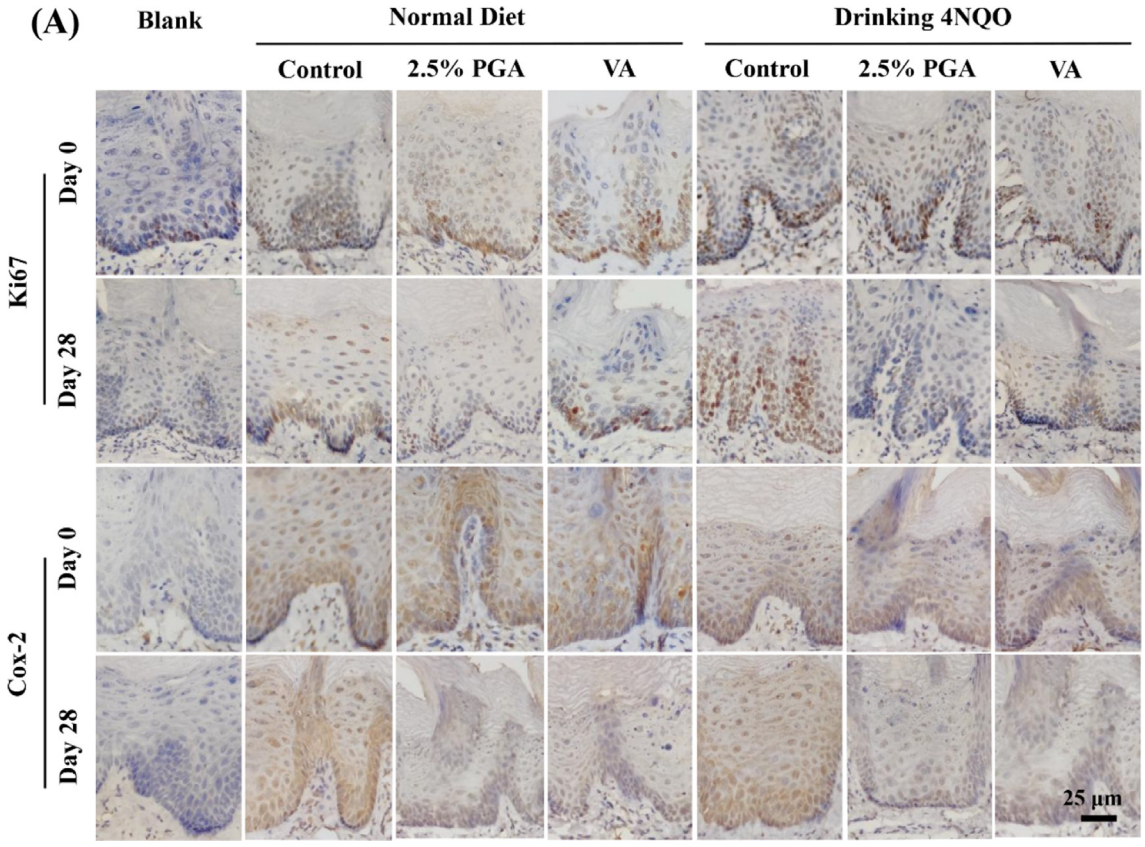

Fig. 6. (A) Immunohistochemical staining with Ki67 and Cox-2 in tongue lesions on the 0 and 28th d. (B) Quantitative analysis of the staining intensity of rat tongue lesions immunohistochemical images on 0 and 28th d. The data are the mean ± SD (*$p < 0.05$, **$p < 0.01$, ***$p < 0.001$).

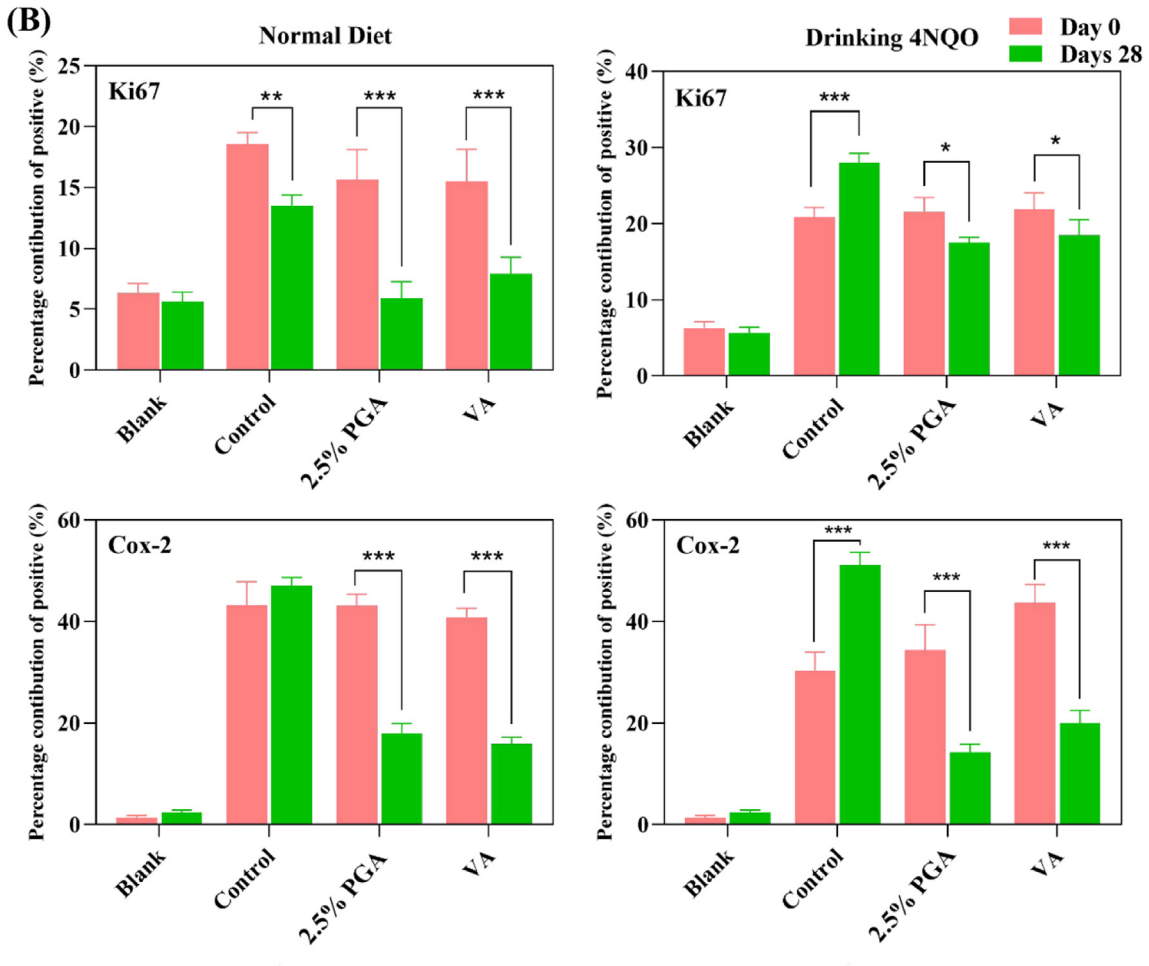

Fig. 6 (*continued*)

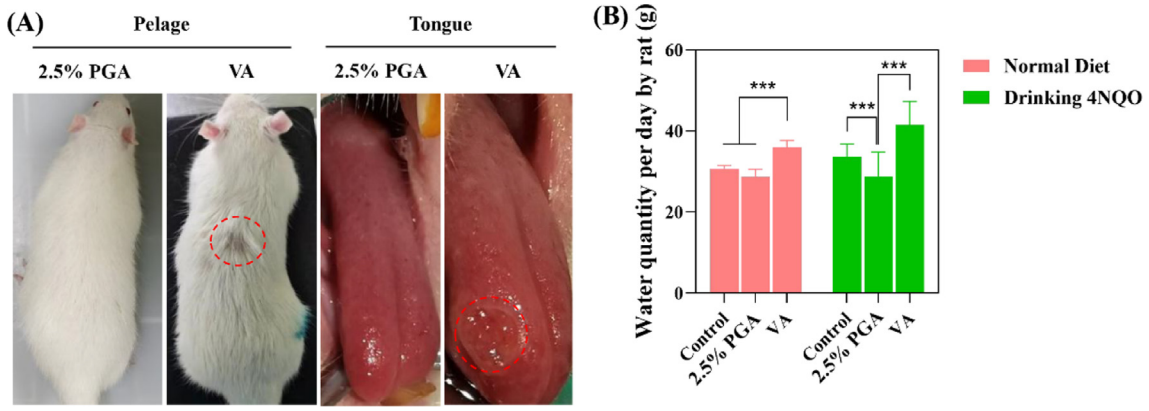

Fig. 7. (A) Photographs of rat fur and tongue mucosa after being treated with 2.5% PGA electrospun membrane and VA ointment for 28 d. (B) Water intake per day of rats. (*$p < 0.05$, **$p < 0.01$, ***$p < 0.001$).

formulation. Significantly, compared to the clinical tretinoin cream formulation, the patches did not induce any side effects (i.e., hair loss and oral ulcers). Therefore, this novel electrospun mucoadhesive bilayer patch displayed great potential for the management of OPL.

Declaration of Competing Interest

The authors declare that they have no known competing financial interests or personal relationships that could have appeared to influence the work reported in this paper.

Acknowledgements

The authors are very grateful for the financial support from the National State Key Laboratory of Oral Diseases Open Fund (Grant No. SKLOD2020OF02), National Natural Science Foundation of China (Grant No. 31900957), Shandong Provincial Natural Science Foundation (Grant No. ZR2019QC007), Innovation and technology program for the excellent youth scholars of higher education of Shandong province (Grant No. 2019KJE015), Traditional Chinese Medicine Science and Technology Project of Shandong province (Grant No. 2021Q069), and the technical support by Pathology Laboratory, School of Stomatology, Qingdao University.

Appendix A. Supplementary data

Supplementary data to this article can be found online at https://doi.org/10.1016/j.matdes.2022.111131.

References

[1] S.H. Sagheer, D. Whitaker-Menezes, J.Y.S. Han, J.M. Curry, U. Martinez-Outschoorn, N.J. Philp, 4NQO induced carcinogenesis: A mouse model for oral squamous cell carcinoma, Methods Cell Biol. 163 (2021) 93–111, https://doi.org/10.1016/bs.mcb.2021.01.001.
[2] B. Wang, S. Zhang, K. Yue, X.D. Wang, The recurrence and survival of oral squamous cell carcinoma : a report of 275 cases, Chin. J. Cancer 32 (2013) 614–618, https://doi.org/10.5732/cjc.012.10219.
[3] M.Z. Mutafchieva, M.N. Draganova-Filipova, P.I. Zagorchev, G.T. Tomov, Oral Lichen Planus - Known and Unknown: a Review, Folia Med. 60 (2018) 528–535, https://doi.org/10.2478/folmed-2018-0017.
[4] V.F. Patel, F. Liu, M.B. Brown, Modeling the oral cavity: In vitro and in vivo evaluations of buccal drug delivery systems, J. Control. Release 161 (3) (2012) 746–756, https://doi.org/10.1016/j.jconrel.2012.05.026.
[5] V.F. Patel, F. Liu, M.B. Brown, Advances in oral transmucosal drug delivery, J. Control. Release 153 (2) (2011) 106–116, https://doi.org/10.1016/j.jconrel.2011.01.027.
[6] M.E. Santocildes-Romero, L. Hadley, K.H. Clitherow, J. Hansen, C. Murdoch, H.E. Colley, M.H. Thornhill, P.V. Hatton, Fabrication of Electrospun Mucoadhesive Membranes for Therapeutic Applications in Oral Medicine, ACS Appl. Mater. Interfaces 9 (13) (2017) 11557–11567, https://doi.org/10.1021/acsami.7b02337.
[7] P. Tonglairoum, T. Ngawhirunpat, T. Rojanarata, S. Panomsuk, R. Kaomongkolgit, P. Opanasopit, Fabrication of mucoadhesive chitosan coated polyvinylpyrrolidone/cyclodextrin/clotrimazole sandwich patches for oral candidiasis, Carbohydr. Polym. 132 (2015) 173–179, https://doi.org/10.1016/j.carbpol.2015.06.032.
[8] A.I. Journal, B. Singh, T. Garg, A.K. Goyal, G. Rath, B. Singh, T. Garg, A.K. Goyal, G. Rath, Development, optimization, and characterization of polymeric electrospun nanofiber : a new attempt in sublingual delivery of nicorandil for the management of angina pectoris Development, optimization, and characterization of polymeric electrospun nano, Artif. Cells, Nanomedicine, Biotechnol. 44 (2016) 1498–1507, https://doi.org/10.3109/21691401.2015.1052472.
[9] C. Dott, C. Tyagi, L.K. Tomar, Y.E. Choonara, P. Kumar, L.C. du Toit, V. Pillay, A Mucoadhesive Electrospun Nanofibrous Matrix for Rapid Oramucosal Drug Delivery, J. Nanomater. 2013 (2013) 1–19, https://doi.org/10.1155/2013/924947.
[10] M. Ren, J. Li, L. Lv, M. Zhang, X. Yang, Q. Zhou, D. Wang, R. Dhakal, Z. Yao, Y. Li, N.-Y. Kim, Wearable and high-performance capacitive pressure sensor based on biocompatible PVP nanofiber membrane via electrospinning and UV treatment, J. Mater. Chem. C (2022), https://doi.org/10.1039/d2tc00955b.
[11] Q. Zhou, J. Xie, M. Bao, H. Yuan, Z. Ye, X. Lou, Y. Zhang, Engineering aligned electrospun PLLA microfibers with nano-porous surface nanotopography for modulating the responses of vascular smooth muscle cells, J. Mater. Chem. B 3 (21) (2015) 4439–4450, https://doi.org/10.1039/c5tb00051c.
[12] Q. Zhou, M. Bao, H. Yuan, S. Zhao, W. Dong, Y. Zhang, Implication of stable jet length in electrospinning for collecting well-aligned ultrafine PLLA fibers, Polymer (Guildf) 54 (25) (2013) 6867–6876, https://doi.org/10.1016/j.polymer.2013.10.042.
[13] Q. Zhang, Y. Ji, W. Zheng, M. Yan, D. Wang, M. Li, J. Chen, X. Yan, Q. Zhang, X. Yuan, Q. Zhou, Electrospun Nanofibers Containing Strontium for Bone Tissue Engineering, J. Nanomater. 2020 (2020) 1257646, https://doi.org/10.1155/2020/1257646.
[14] L. Yang, S. Pijuan-Galito, H.S. Rho, A.S. Vasilevich, A.D. Eren, L.u. Ge, P. Habibović, M.R. Alexander, J. de Boer, A. Carlier, P. van Rijn, Q. Zhou, High-Throughput Methods in the Discovery and Study of Biomaterials and Materiobiology, Chem. Rev. 121 (8) (2021) 4561–4677, https://doi.org/10.1021/acs.chemrev.0c00752.
[15] A. Martins, R.L. Reis, N.M. Neves, Electrospinning: Processing technique for tissue engineering scaffolding, Int. Mater. Rev. 53 (5) (2008) 257–274, https://doi.org/10.1179/174328008X353547.
[16] Y.-F. Goh, I. Shakir, R. Hussain, Electrospun fibers for tissue engineering, drug delivery, and wound dressing, J. Mater. Sci. 48 (8) (2013) 3027–3054, https://doi.org/10.1007/s10853-013-7145-8.
[17] A.A. Aldana, G.A. Abraham, Current advances in electrospun gelatin-based scaffolds for tissue engineering applications, Int. J. Pharm. 523 (2) (2017) 441–453, https://doi.org/10.1016/j.ijpharm.2016.09.044.
[18] Q. Zhou, H. Zhang, Y.a. Zhou, Z. Yu, H. Yuan, B. Feng, P. van Rijn, Y. Zhang, Alkali-Mediated Miscibility of Gelatin/Polycaprolactone for Electrospinning Homogeneous Composite Nanofibers for Tissue Scaffolding, Macromol. Biosci. 17 (12) (2017) 1700268, https://doi.org/10.1002/mabi.201700268.
[19] Y. Zhang, H. Ouyang, C.T. Lim, S. Ramakrishna, Z.-M. Huang, Electrospinning of gelatin fibers and gelatin/PCL composite fibrous scaffolds, J. Biomed. Mater. Res. B. Appl. Biomater. 72B (1) (2005) 156–165, https://doi.org/10.1002/jbm.b.30128.
[20] E. Chong, T. Phan, I. Lim, Y. Zhang, B. Bay, S. Ramakrishna, C. Lim, Evaluation of electrospun PCL/gelatin nanofibrous scaffold for wound healing and layered dermal reconstitution, Acta Biomater. 3 (3) (2007) 321–330, https://doi.org/10.1016/j.actbio.2007.01.002.
[21] X. Yang, F. Yang, X.F. Walboomers, Z. Bian, M. Fan, J.A. Jansen, The performance of dental pulp stem cells on nanofibrous PCL/gelatin/nHA scaffolds, J. Biomed. Mater. Res. - Part A. 93 (2010) 247–257, https://doi.org/10.1002/jbm.a.32535.
[22] M.A. Alvarez-Perez, V. Guarino, V. Cirillo, L. Ambrosio, Influence of gelatin cues in PCL electrospun membranes on nerve outgrowth, Biomacromolecules 11 (9) (2010) 2238–2246, https://doi.org/10.1021/bm100221h.
[23] O. Hartman, C. Zhang, E.L. Adams, M.C. Farach-Carson, N.J. Petrelli, B.D. Chase, J.F. Rabolt, Biofunctionalization of electrospun PCL-based scaffolds with perlecan domain IV peptide to create a 3-D pharmacokinetic cancer model, Biomaterials 31 (21) (2010) 5700–5718, https://doi.org/10.1016/j.biomaterials.2010.03.017.
[24] K. Gauthaman, J.R. Venugopal, F.C. Yee, G.S.L. Peh, S. Ramakrishna, A. Bongso, Nanofibrous substrates support colony formation and maintain stemness of human embryonic stem cells, J. Cell. Mol. Med. 13 (2009) 3475–3484, https://doi.org/10.1111/j.1582-4934.2009.00699.x.
[25] V.P. Nguyen, S. Park, J. Oh, H. Wook Kang, Wook Kang, Biocompatible astaxanthin as novel contrast agent for biomedical imaging, J. Biophotonics 10 (8) (2017) 1053–1061, https://doi.org/10.1002/jbio.201600159.
[26] Y. Zhou, J.S. Baker, X. Chen, Y. Wang, H. Chen, G.W. Davison, X. Yan, High-dose astaxanthin supplementation suppresses antioxidant enzyme activity during moderate-intensity swimming training in mice, Nutrients 11 (2019) 1–13, https://doi.org/10.3390/nu11061244.
[27] L. Ekpe, K. Inaku, E. Eyam, V. Ekpe, Antioxidant Effects of Astaxanthin in Various Diseases - a Review, Oxid. Antioxid. Med. Sci. 7 (2018) 1, https://doi.org/10.5455/oams.20180315075538.
[28] Y.T. Chen, C.J. Kao, H.Y. Huang, S.Y. Huang, C.Y. Chen, Y.S. Lin, Z.H. Wen, H.M.D. Wang, Astaxanthin reduces MMP expressions, suppresses cancer cell migrations, and triggers apoptotic caspases of in vitro and in vivo models in melanoma, J. Funct. Foods. 31 (2017) 20–31, https://doi.org/10.1016/j.jff.2017.01.005.
[29] J. Zhang, Z. Sun, P. Sun, T. Chen, F. Chen, Microalgal carotenoids: Beneficial effects and potential in human health, Food Funct. 5 (2014) 413–425, https://doi.org/10.1039/c3fo60607d.
[30] R.R. Ambati, P.S. Moi, S. Ravi, R.G. Aswathanarayana, Astaxanthin: Sources, extraction, stability, biological activities and its commercial applications - A review, Mar. Drugs 12 (2014) 128–152, https://doi.org/10.3390/md12010128.
[31] J.-P. Yuan, J. Peng, K. Yin, J.-H. Wang, Potential health-promoting effects of astaxanthin: A high-value carotenoid mostly from microalgae, Mol. Nutr. Food Res. 55 (1) (2011) 150–165, https://doi.org/10.1002/mnfr.201000414.
[32] K. Bouchemal, S. Briançon, E. Perrier, H. Fessi, Nano-emulsion formulation using spontaneous emulsification: Solvent, oil and surfactant optimisation, Int. J. Pharm. 280 (1-2) (2004) 241–251, https://doi.org/10.1016/j.ijpharm.2004.05.016.
[33] K. Kavitha, J. Kowshik, T.K.K. Kishore, A.B. Baba, S. Nagini, Astaxanthin inhibits NF-κB and Wnt/β-catenin signaling pathways via inactivation of Erk/MAPK and PI3K/Akt to induce intrinsic apoptosis in a hamster model of oral cancer, Biochim. Biophys. Acta - Gen. Subj. 1830 (10) (2013) 4433–4444, https://doi.org/10.1016/j.bbagen.2013.05.032.
[34] J. Kowshik, A.B. Baba, H. Giri, G. Deepak Reddy, M. Dixit, S. Nagini, S.R. Singh, Astaxanthin inhibits JAK/STAT-3 signaling to abrogate cell proliferation, invasion and angiogenesis in a hamster model of oral cancer, PLoS One 9 (10) (2014) e109114, https://doi.org/10.1371/journal.pone.0109114.
[35] M.-R. Cho, J.-H. Han, H.-J. Lee, Y.K. Park, M.-H. Kang, Emerging functional cross?talk Kyoto, Japbn.14-134 0912-5086 Original Article Journal of Clinical Biochemistry and Nutrition JCBNcbn14-13c4 10.3164/jj1880 0009athe Society for Free Radical Research Japan between the Keap1?Nrf2 system and mitochondria, J. Clin. Biochem. Nutr. 56 (2015) 49–56. doi:10.3164/jcbn.14.
[36] M. Zare, Z. Norouzi Roshan, E. Assadpour, S.M. Jafari, Improving the cancer prevention/treatment role of carotenoids through various nano-delivery systems, Crit. Rev. Food Sci. Nutr. 61 (3) (2021) 522–534, https://doi.org/10.1080/10408398.2020.1738999.
[37] R. Koshani, S.M. Jafari, Ultrasound-assisted preparation of different nanocarriers loaded with food bioactive ingredients, Adv. Colloid Interface Sci. 270 (2019) 123–146, https://doi.org/10.1016/j.cis.2019.06.005.

[38] H. Rostamabadi, S.R. Falsafi, S.M. Jafari, Nanoencapsulation of carotenoids within lipid-based nanocarriers, J. Control. Release 298 (2019) 38–67, https://doi.org/10.1016/j.jconrel.2019.02.005.
[39] W. Pothitirat, M.T. Chomnawang, R. Supabphol, W. Gritsanapan, Fitoterapia Comparison of bioactive compounds content, free radical scavenging and anti-acne inducing bacteria activities of extracts from the mangosteen fruit rind at two stages of maturity, Fitoterapia 80 (7) (2009) 442–447, https://doi.org/10.1016/j.fitote.2009.06.005.
[40] A. Figueiras, J. Hombach, F. Veiga, A. Bernkop-Schnürch, In vitro evaluation of natural and methylated cyclodextrins as buccal permeation enhancing system for omeprazole delivery, Eur. J. Pharm. Biopharm. 71 (2) (2009) 339–345, https://doi.org/10.1016/j.ejpb.2008.08.016.
[41] X. Qiu, S. Xu, Y. Hao, B. Peterson, B. Li, K. Yang, X. Lv, Q. Zhou, Q. Ji, Colloids and Surfaces B : Biointerfaces Biological e ff ects on tooth root surface topographies induced by various mechanical treatments, Colloids Surf. B Biointerfaces 188 (2020) 110748, https://doi.org/10.1016/j.colsurfb.2019.110748.
[42] J.Y. Lai, Y.T. Li, C.H. Cho, T.C. Yu, Nanoscale modification of porous gelatin scaffolds with chondroitin sulfate for corneal stromal tissue engineering, Int. J. Nanomed. 7 (2012) 1101–1114, https://doi.org/10.2147/IJN.S28753.
[43] M. Bin Ahmad, J.J. Lim, K. Shameli, N.A. Ibrahim, M.Y. Tay, Synthesis of silver nanoparticles in chitosan, gelatin and chitosan/gelatin bionanocomposites by a chemical reducing agent and their characterization, Molecules 16 (2011) 7237–7248, https://doi.org/10.3390/molecules16097237.
[44] M. Balietti, S.R. Giannubilo, B. Giorgetti, M. Solazzi, A. Turi, T. Casoli, A. Ciavattini, P. Fattorettia, The effect of astaxanthin on the aging rat brain: Gender-related differences in modulating inflammation, J. Sci. Food Agric. 96 (2016) 615–618, https://doi.org/10.1002/jsfa.7131.
[45] A. Ligia Focsan, N.E. Polyakov, L.D. Kispert, Supramolecular carotenoid complexes of enhanced solubility and stability — The way of bioavailability improvement, Molecules 24 (2019), https://doi.org/10.3390/molecules24213947.
[46] H. Rostamabadi, S.R. Falsafi, S.M. Jafari, SC, Trends Food Sci. Technol. (2019). doi:10.1016/j.tifs.2019.04.004.
[47] MohammadReza Rostami, M. Yousefi, A. Khezerlou, M. Aman Mohammadi, S. M. Jafari, Application of different biopolymers for nanoencapsulation of antioxidants via electrohydrodynamic processes, Food Hydrocoll. 97 (2019) 105170, https://doi.org/10.1016/j.foodhyd.2019.06.015.
[48] H. Ravi, N. Kurrey, Y. Manabe, T. Sugawara, V. Baskaran, Polymeric chitosan-glycolipid nanocarriers for an effective delivery of marine carotenoid fucoxanthin for induction of apoptosis in human colon cancer cells (Caco-2 cells), Mater. Sci. Eng. C. 91 (2018) 785–795, https://doi.org/10.1016/j.msec.2018.06.018.
[49] I. Katouzian, S.M. Jafari, Protein nanotubes as state-of-the-art nanocarriers: Synthesis methods, simulation and applications, J. Control. Release 303 (2019) 302–318, https://doi.org/10.1016/j.jconrel.2019.04.026.
[50] I. Higuera-Ciapara, L. Félix-Valenzuela, F.M. Goycoolea, Astaxanthin: A review of its chemistry and applications, Crit. Rev. Food Sci. Nutr. 46 (2) (2006) 185–196, https://doi.org/10.1080/10408690590957188.
[51] C. Yang, Z. Yan, Y. Lian, J. Wang, K. Zhang, Graphene oxide coated shell-core structured chitosan/PLLA nanofibrous scaffolds for wound dressing, J. Biomater. Sci. Polym. Ed. 31 (5) (2020) 622–641, https://doi.org/10.1080/09205063.2019.1706149.
[52] Y. Nishio, R.S.T.J. Manley, Blends of Cellulose With Nylon 6 and Poly (4aprolactone) Prepared by a Solution-Coagulation Method, Polym. Eng. Sci. 30 (1990) 71–82, https://doi.org/10.1002/pen.760300203.
[53] M. Bao, X. Lou, Q. Zhou, W. Dong, H. Yuan, Y. Zhang, Electrospun biomimetic fibrous scaffold from shape memory polymer of PDLLA- co -TMC for bone tissue engineering, ACS Appl. Mater. Interfaces 6 (4) (2014) 2611–2621, https://doi.org/10.1021/am405101k.
[54] W. Zheng, Y. Hao, D. Wang, H. Huang, F. Guo, Z. Sun, P. Shen, K. Sui, C. Yuan, Q. Zhou, Preparation of triamcinolone acetonide-loaded chitosan / fucoidan hydrogel and its potential application as an oral mucosa patch, Carbohydr. Polym. 272 (2021) 118493, https://doi.org/10.1016/j.carbpol.2021.118493.
[55] S. Xu, Q. Zhou, Z. Jiang, Y. Wang, K. Yang, X. Qiu, Q. Ji, The effect of doxycycline-containing chitosan/carboxymethyl chitosan nanoparticles on NLRP3 inflammasome in periodontal disease, Carbohydr. Polym. 237 (2020) 116163.
[56] H. Qi, J. Yang, J. Yu, L. Yang, P. Shan, S. Zhu, Y. Wang, P. Li, Glucose - responsive nanogels efficiently maintain the stability and activity of therapeutic enzymes, (2022) 1511–1524. doi.org/10.1515/ntrev-2022-0095
[57] T.J. Sill, H.A. von Recum, Electrospinning: applications in drug delivery and tissue engineering, Biomaterials. 29 (2008) 1989–2006, https://doi.org/10.1016/j.biomaterials.2008.01.011.
[58] Z.K. Nagy, K. Nyul, I. Wagner, K. Molnar, G.y. Marosi, Electrospun water soluble polymer mat for ultrafast release of Donepezil HCl, EXPRESS Polym. Lett. 4 (12) (2010) 763–772, https://doi.org/10.3144/expresspolymlett.2010.92.
[59] Y. Sudhakar, K. Kuotsu, A.K. Bandyopadhyay, Buccal bioadhesive drug delivery — A promising option for orally less efficient drugs, J. Control. Release 114 (1) (2006) 15–40, https://doi.org/10.1016/j.jconrel.2006.04.012.
[60] J. Xu, S. Strandman, J.X.X. Zhu, J. Barralet, M. Cerruti, Biomaterials Genipin-crosslinked catechol-chitosan mucoadhesive hydrogels for buccal drug delivery, Biomaterials. 37 (2015) 395–404, https://doi.org/10.1016/j.biomaterials.2014.10.024.
[61] V.V. Khutoryanskiy, Advances in Mucoadhesion and Mucoadhesive Polymers, Macromol. Biosci. 11 (6) (2011) 748–764, https://doi.org/10.1002/mabi.201000388.
[62] Y. Hao, W. Zheng, Z. Sun, D. Zhang, K. Sui, P. Shen, P. Li, Q. Zhou, Marine polysaccharide-based composite hydrogels containing fucoidan: Preparation, physicochemical characterization, and biocompatible evaluation, Int. J. Biol. Macromol. 183 (2021) 1978–1986, https://doi.org/10.1016/j.ijbiomac.2021.05.190.
[63] Y. Ji, Z. Han, H. Ding, X. Xu, D. Wang, Y. Zhu, F. An, S. Tang, H. Zhang, J. Deng, Q. Zhou, Enhanced Eradication of Bacterial/Fungi Biofilms by Glucose Oxidase-Modified Magnetic Nanoparticles as a Potential Treatment for Persistent Endodontic Infections, ACS Appl. Mater. Interfaces. 13 (15) (2021) 17289–17299, https://doi.org/10.1021/acsami.1c01748.
[64] Y. Hao, W. Zhao, H. Zhang, W. Zheng, Q. Zhou, Carboxymethyl chitosan-based hydrogels containing fibroblast growth factors for triggering diabetic wound healing, Carbohydr. Polym. 287 (2022) 119336, https://doi.org/10.1016/j.carbpol.2022.119336.
[65] M. Yan, Y. Pan, S. Lu, X. Li, D. Wang, T. Shao, Z. Wu, Q. Zhou, Chitosan-CaP microflowers and metronidazole loaded calcium alginate sponges with enhanced antibacterial, hemostatic and osteogenic properties for the prevention of dry socket after tooth removal, Int. J. Biol. Macromol. 212 (2022) 134–145. doi:org/10.1016/j.ijbiomac.2022.05.094.
[66] R.G. Flemming, C.J. Murphy, G.A. Abrams, S.L. Goodman, P.F. Nealey, Effects of synthetic micro- and nano-structured surfaces on cell behavior, Biomaterials 20 (6) (1999) 573–588, https://doi.org/10.1016/S0142-9612(98)00209-9.
[67] A.F.V.O.N. Recum, D. Ph, C.E. Shannon, C.E. Cannon, K.J. Long, T.G.V.A.N. Kooten, D. Ph, J. Meyle, D. Ph, Modifiers of Cellular Adhesion, Tissue Eng. 2 (1996) 241–253, https://doi.org/10.1089/ten.1996.2.241.
[68] A.M. Green, J.A. Jansen, A.F. Von Recum, Fibroblast response to microtextured silicone surfaces : Texture orientation into or out of the surface, J. Biomed. Mater. Res. 28 (1994) 647–653, https://doi.org/10.1002/jbm.820280515.
[69] R.K. Rajan, S. Chandran, H.V. Sreelatha, A. John, R. Parameswaran, Pamidronate-Encapsulated Electrospun Polycaprolactone-Based Composite Scaffolds for Osteoporotic Bone Defect Repair, ACS Appl. Bio Mater. 3 (4) (2020) 1924–1933, https://doi.org/10.1021/acsabm.9b01077.
[70] B.S. and J. H.ElISSEEFF, Engineering Structurally Organized Cartilage and Bone Tissues, Ann. OfBiomedical Eng. 32 (2004) 148–159. doi:10.1023/B:ABME.0000007799.60142.7.
[71] X. Li, W. Li, G. Ma, X. Liang, J. Xiao, R. Jacobs, Original Oral Cavity Carcinogenesis Modeled in Carcinogen-Treated Mice, J. Hard Tissue Biol. 22 (4) (2013) 425–432, https://doi.org/10.2485/jhtb.22.425.
[72] L. Cao, J.A. Werkmeister, J. Wang, V. Glattauer, K.M. McLean, C. Liu, Biomaterials Bone regeneration using photocrosslinked hydrogel incorporating rhBMP-2 loaded 2-N, 6-O- sulfated chitosan nanoparticles, Biomaterials 35 (9) (2014) 2730–2742, https://doi.org/10.1016/j.biomaterials.2013.12.028.
[73] A. Takkem, C. Barakat, S. Zakarea, K. Zaid, J. Najmeh, M. Ayoub, M.Y. Seirawan, Ki-67 Prognostic Value in Different Histological Grades of Oral Epithelial Dysplasia and Oral Squamous Cell Carcinoma, Asian Pacific, J. Cancer Prev. 19 (11) (2018) 3279–3286, https://doi.org/10.31557/APJCP.2018.19.11.3279.
[74] B.M. Erovic, M. Pelzmann, D. Turhani, J. Pammer, V. Niederberger, C. Neuchrist, M.C. Grasl, D. Thurnher, Acta Oto-Laryngologica Differential Expression Pattern of Cyclooxygenase-1 and -2 in Head and Neck Squamous Cell Carcinoma, Acta Otolaryngol. 123 (8) (2003) 950–953, https://doi.org/10.1080/00016480310016118.
[75] M. Shibata, I. Kodani, M. Osaki, K. Araki, H. Adachi, K. Ryoke, H. Ito, Cyclo-oxygenase-1 and -2 expression in human oral mucosa, dysplasias and squamous cell carcinomas and their pathological significance, Oral Oncol. 41 (3) (2005) 304–312, https://doi.org/10.1016/j.oraloncology.2004.09.009.
[76] H. Antônio, R. Pontes, F. Sirotheau, C. Pontes, F.P. Fonseca, P.L. De Carvalho, É. M. Pereira, M.C. De Abreu, B. Santos, D.F. Silva, S. Pinto, J. Dds, Annals of Diagnostic Pathology Nuclear factor κ B and cyclooxygenase-2 immunoexpression in oral dysplasia and oral squamous cell carcinoma ☆, Ann. Diagn. Pathol. 17 (2013) 45–50, https://doi.org/10.1016/j.anndiagpath.2012.04.008.
[77] G. Ozgun, S. Senturk, S. Erkek-Ozhan, Retinoic acid signaling and bladder cancer: Epigenetic deregulation, therapy and beyond, Int. J. Cancer 148 (10) (2021) 2364–2374, https://doi.org/10.1002/ijc.33374.
[78] S. Khalil, T. Bardawil, C. Stephan, N. Darwiche, O. Abbas, A.G. Kibbi, G. Nemer, M. Kurban, Retinoids: a journey from the molecular structures and mechanisms of action to clinical uses in dermatology and adverse effects, J. Dermatolog. Treat. 28 (8) (2017) 684–696, https://doi.org/10.1080/09546634.2017.1309349.
[79] K. Murata, A. Oyagi, D. Takahira, K. Tsuruma, M. Shimazawa, T. Ishibashi, H. Hara, Protective Effects of Astaxanthin from Paracoccus carotinifaciens on Murine Gastric Ulcer Models, Phyther. Res. 26 (8) (2012) 1126–1132, https://doi.org/10.1002/ptr.3681.